

The effect of proppant size on hydraulic fracturing by a slurry



Dontsov, E.V. and Peirce, A.P.

University of British Columbia, Vancouver, BC, Canada

Copyright 2014 ARMA, American Rock Mechanics Association

This paper was prepared for presentation at the 48th US Rock Mechanics / Geomechanics Symposium held in Minneapolis, MN, USA, 1-4 June 2014.

This paper was selected for presentation at the symposium by an ARMA Technical Program Committee based on a technical and critical review of the paper by a minimum of two technical reviewers. The material, as presented, does not necessarily reflect any position of ARMA, its officers, or members. Electronic reproduction, distribution, or storage of any part of this paper for commercial purposes without the written consent of ARMA is prohibited. Permission to reproduce in print is restricted to an abstract of not more than 200 words; illustrations may not be copied. The abstract must contain conspicuous acknowledgement of where and by whom the paper was presented.

ABSTRACT: Proppant additives play an essential role in hydraulic fracturing as they provide support, which retains the fracture opening after the pumping is shut off. From a production point of view, a larger proppant size provides better permeability, while, at the same time, gravitational settling may cause significant distortion of the particle distribution inside the fracture for heavier particles. This study uses a recently developed model for proppant transport, that has been implemented for Khristianovich-Zhel'tov-Geertsma-De Klerk (KGD) and pseudo-3D (P3D) fracture geometries, to quantify the effect of particle settling. The proppant transport model is based on an empirical constitutive relation for the slurry that accounts for: i) a non-uniform particle distribution across the fracture width due to shear-induced migration, which distorts the parabolic velocity profile, ii) slip velocity in the direction of flow, which, in the limit of a jammed state, leads to Darcy's law, and iii) gravitational settling. While the gravitational settling is the biggest concern when dealing with larger particle sizes, other effects may include earlier jamming due to proppant stalling in between the walls and higher permeability of the proppant plug, which promotes the fracture propagation in front of the jammed region.

1. INTRODUCTION

Hydraulic fracturing is an irreplaceable tool for the oil and gas industry, as it enables one to fracture the rock below the ground surface producing high conductivity channels for better production rates. To advance an initially perforated zone, pressurized fluid is pumped methodically into the opening, inducing fracture growth. One of the key aspects in using hydraulic fracturing is the possibility to maintain the fracture opening after pumping by injecting particles or proppant together with the fracturing fluid [1]. The fact that the slurry, i.e. the mixture of the fracturing fluid and the particles, is used for fracturing introduces numerous research objectives, including but not limited to: i) the study of the viscous properties of the slurry [2], ii) numerical modelling and experimental observation of proppant transport and settling [3, 4, 5], iii) generating a proppant pumping schedule [6, 7, 8], iv) calculating the residual fracture opening after the pumping is shut off [9], and v) studying flowback within the hydraulic fractures [10, 11].

Selecting an appropriate proppant size for a given hydraulic fracturing job is another challenging question.

Clearly, bigger particles lead to higher permeability and consequently to better production rates. At the same time, gravitational settling of the proppant increases dramatically with the particle size and can significantly affect proppant placement inside the fracture. These opposing mechanisms are the primary factors that determine the optimal particle size. However, the effects of the proppant size are not limited to the aforementioned phenomena. In particular, bigger particles may not reach the crack tip region since they could stick between the fracture walls a long way from the tip. In addition, in situations when crack tip screen-out is achieved, the permeability of the proppant plug is directly affected by the particle size, so that the fracture could be either arrested (for small particles) or not (for bigger particles), which can have a significant impact on the final fracture footprint.

The main purpose of this study is to try to quantify the particle size effects in hydraulic fracturing by means of numerical modelling. The approach is built on the proppant transport model developed in [5], which is capable of capturing gravitational settling, as well as proppant plug formation, growth, and fluid filtration through it. To help understand the features of the proppant transport model,

Section 2 briefly summarizes its capabilities and limitations. Then, the numerical scheme, adopted from [5], is utilized in Sections 3 and 4 to study the particle size effects for KGD and P3D fracture geometries, respectively.

2. PROPPANT TRANSPORT MODEL DESCRIPTION

This section aims to describe the proppant transport model, introduced in [5], which will be used for the analysis of the proppant size effects. One of the key ingredients of the model is the constitutive framework for the slurry, i.e. the variation of the shear and normal stresses with shear rate and concentration of the particles. To come up with a more realistic model, empirical constitutive relations, established in [12], are adopted. Note that the particle size does not enter the problem via these constitutive relations, instead, it appears in the viscous interaction force between the phases and in the gravitational term. In addition, the particles are assumed to be spherical and monodisperse, i.e. all of the same size. Equipped with the appropriate constitutive framework, the problem of a steady slurry flow in a channel is analyzed, providing solutions for both the velocity profile and the particle distribution across the channel for different average proppant volume fractions. Several distinct features of the solution include a blunted velocity profile, which becomes more uniform for higher concentrations, as well as a higher particle concentration near the centre of the channel where the shear rates are the smallest. Moreover, it is shown that the particles form a rigid plug at the centre, whose size increases with the average particle concentration. To relate the examined solutions to a hydraulic fracturing problem, average fluxes of the slurry and the particles are calculated by integrating the appropriate velocity profiles. These fluxes are then used to formulate the governing equations for the slurry and proppant transport inside the fracture, namely the corresponding volume balances, as

$$\begin{aligned} \frac{\partial w}{\partial t} + \nabla \cdot \mathbf{q}^s + g &= Q, \\ \frac{\partial w \bar{\phi}}{\partial t} + \nabla \cdot \mathbf{q}^p &= \bar{\phi}_0 Q, \end{aligned} \quad (1)$$

where w is the width of the fracture, g is the leak-off term (Carter's leak-off model is used [13]), Q is the source term, $\bar{\phi}$ is the average particle concentration that is normalized by the maximum value $\phi_m = 0.585$ (i.e. $0 \leq \bar{\phi} \leq 1$), $\bar{\phi}_0$ is the normalized input proppant concentration, while \mathbf{q}^s and \mathbf{q}^p are the aforementioned slurry and prop-

ant fluxes, given respectively by

$$\begin{aligned} \mathbf{q}^s &= -\frac{w^3}{12\mu^f} Q^s(\bar{\phi}) \nabla p - \frac{a^2 w}{12\mu^f} D(\bar{\phi}) \nabla p, \\ \mathbf{q}^p &= -B\left(\frac{w}{a}\right) \frac{w(w^2 - w_{cr}^2(\bar{\phi}))}{12\mu^f} Q^p(\bar{\phi}) \nabla p \quad (2) \\ &\quad + B\left(\frac{w}{a}\right) B_g(\bar{\phi}) \frac{a^2 w}{12\mu^f} (\rho^p - \rho^f) G(\bar{\phi}) \mathbf{g}. \end{aligned}$$

Here μ^f is the viscosity of the clear fluid, p is the fluid pressure, a denotes the particle radius, \mathbf{g} is the gravitational acceleration, $\rho^p - \rho^f$ is the difference between particle and fluid mass densities, functions $Q^s(\bar{\phi})$, $D(\bar{\phi})$, $Q^p(\bar{\phi})$, $w_{cr}(\bar{\phi})$ and $G(\bar{\phi})$ are computed numerically using the solution for a steady flow in a channel, while $B(w/a)$ and $B_g(\bar{\phi})$ are the ‘‘blocking’’ functions. To better understand the characteristics of the fluxes, Fig. 1 shows the variations of the functions Q^s , D , Q^p , w_{cr} and G versus $\bar{\phi}$. The top row shows the functions that enter the slurry flux, \mathbf{q}^s , while the bottom row shows the functions that affect the proppant flux, \mathbf{q}^p . As can be seen from equation (2a), the slurry flux has two distinct terms, one that represents Poiseuille's law with the inverse of Q^s being related to effective viscosity, and another that represents filtration or Darcy's law, with D being related to the intrinsic permeability. Indeed, according to Fig. 1, $Q^s \approx 1$ and $D \approx 0$ for low particle concentrations, so that the slurry flows according to Poiseuille's law. At the same time, $Q^s \approx 0$ for high concentrations, while D stays finite, which implies that the slurry is transported primarily by means of fluid filtration through a dense particle agglomerate. Note that the particle radius enters the ‘‘filtration’’ term in (2a), and thus may influence the hydraulic fracture propagation in situations when the particle concentrations are in a close proximity to the maximum value, e.g. when a crack tip screen-out is achieved. The proppant flux, \mathbf{q}^p , also has two distinct terms, one related to the fact that the particles are carried forward by the viscous fluid, and another due to gravitational settling. The function Q^p in Fig. 1 shows that the particle flux is small for both low and high concentrations, because there are either few particles to transport or the effective viscosity is so high that the particles can hardly be moved. Function w_{cr} introduces a critical width for which the particle flux vanishes according to the model. Unfortunately, its values are always below 2, where the latter corresponds to the width equal to the particle diameter. To prevent particle placement in the narrow regions with $w < 2a$, the ‘‘blocking’’ function B is introduced. This function gradually reduces the proppant flux to zero, as particles approach a narrow channel. The second term in the proppant flux in (2b) is related to gravitational settling. As indicated in Fig. 1, the flux due to settling first increases with the particle volume fraction,

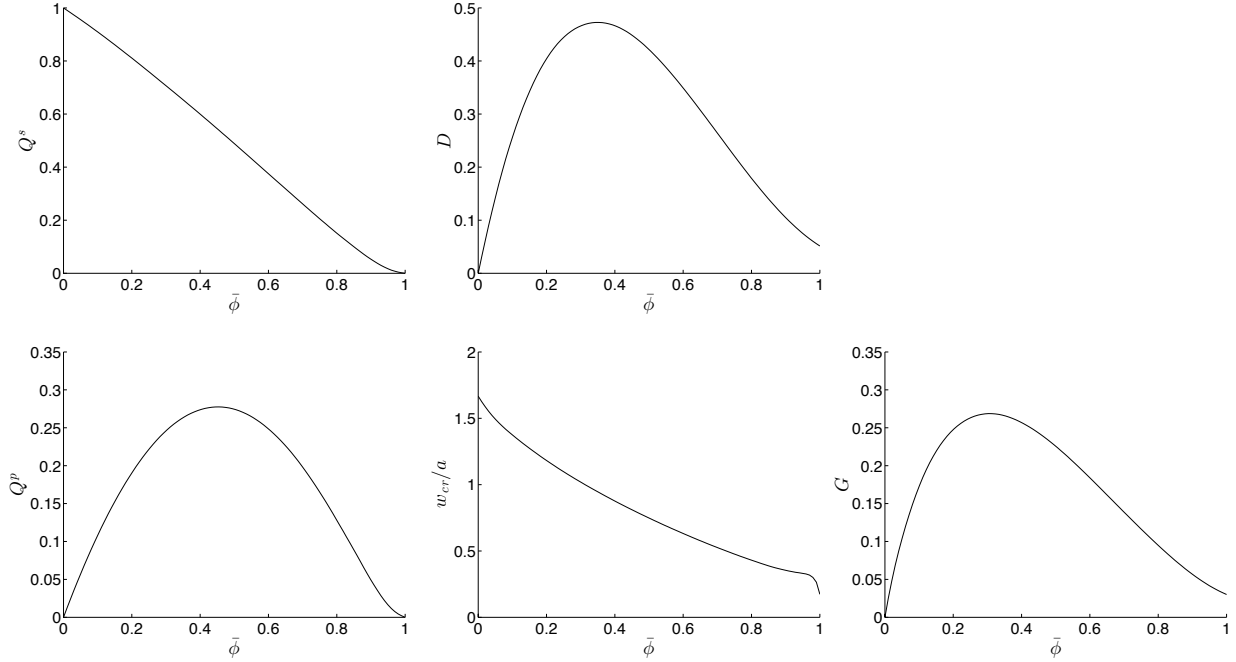


Figure 1: Variation of the functions Q^s , D , Q^p , w_{cr} and G versus $\bar{\phi}$.

but then it starts to decrease since the particles begin to interact at higher concentrations, which slows the settling velocity. Note that even for the maximum concentration, there is a finite settling velocity, which is related to both the fact that the slip velocity between the phases does not vanish even for the maximum concentration, and the way the gravitational settling is introduced in [5]. If one considers solely the settling of the particles (without a pressure gradient), then such a configuration would lead to concentrations that exceed the maximum value allowed. To resolve this issue, the “blocking” function B_g is introduced. This function forces the proppant flux due to settling to vanish continuously for volume fractions approaching the maximum value. As indicated in [5], for the purpose of numerical computations, B and B_g are chosen as

$$B\left(\frac{w}{a}\right) = H\left(\frac{w}{a} - 2\right) \min\left\{1, \frac{\frac{w}{a} - 2}{\frac{w}{a_{bl}} - 2}\right\}, \quad (3)$$

$$B_g(\bar{\phi}) = \min\left\{1, \frac{1 - \bar{\phi}}{1 - \bar{\phi}_{bl}}\right\},$$

where $w_{bl} = 2.5a$ and $\bar{\phi}_{bl} = 0.95$. With the above discussion about the “blocking” functions, it seems that the function w_{cr} does not introduce a noticeable contribution to the proppant transport, while, at the same time, both the “blocking” function B and the gravitational settling may significantly affect the particle placement inside the fracture. The first arrests particles before the fracture tip, which could potentially lead to premature tip screen-out, while the second induces asymmetry in the proppant placement, which could also affect the fracture propagation. Both effects are related to the proppant size, and

their consequences will be analyzed in Sections 3 and 4.

3. EFFECTS FOR KGD FRACTURES

This section utilizes a numerical algorithm for a hydraulic fracture driven by a slurry [5] to study proppant size effects for the KGD fracture geometry. It should be noted that, in addition to (1), the hydraulic fracturing problem must be complemented by the elasticity equation and appropriate boundary conditions, see [5] for details. To investigate the effects associated solely with the particle size, one reference fracture configuration is analyzed, i.e. all the parameters are held fixed except for the particle properties. The numerical simulations in this section start at $t_{\text{start}} = 1$ s, assuming initial left and right half-lengths equal to $l_1 = l_2 = 1$ m, and an elliptic opening with a maximum width $w_{\text{max}} = 5 \times 10^{-4}$ m. Pure fluid is used to propagate the fracture until $t_p = 1000$ s, after which the proppant is introduced, so that for $t > t_p$, the slurry is pumped. The pumping ends at $t_{\text{end}} = 4000$ s. This represents a very simplified proppant schedule, which is used for illustrative purposes, while there are other possibilities to construct more effective schedules [6, 7, 8]. The input volume concentration of particles is taken to be $\bar{\phi}_0 = 0.2$, but note that $\bar{\phi}_0$ is the normalized concentration, so that the true concentration is $\phi_m \bar{\phi}_0$, where $\phi_m = 0.585$. Other parameters used for the calculations are $E' = E/(1 - \nu^2) = 25 \times 10^9$ Pa for the plane strain modulus, $\mu^f = 0.1$ Pa·s for the intrinsic fluid viscosity, $Q_0 = 10^{-4}$ m²/s for the inlet flux, $C' = 5 \times 10^{-5}$ m/s^{1/2} for the leak-off coefficient, and $K_{1c} = 10^6$ Pa·m^{1/2} for the

fracture toughness. The problem also accounts for stress barriers, located symmetrically at $l_\sigma = 10$ m from the inlet, with a magnitude $\Delta\sigma = 2.5 \times 10^6$ Pa. Various particle radii in the range $0.2 \leq a \leq 0.8$ mm are used. Both buoyant and weighted particles are considered. For the latter case, the difference in the mass densities between the proppant and the fluid is taken as $\rho^p - \rho^f = 1300$ kg/m³, while the gravitational acceleration is set to $g = 9.8$ m/s².

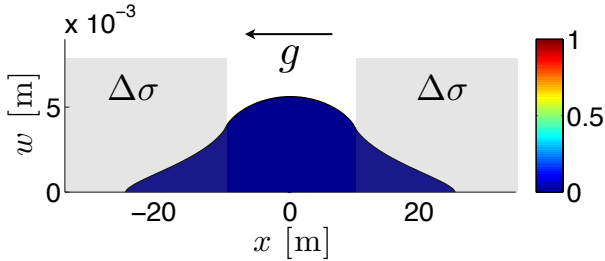


Figure 2: Variation of the width of the fracture versus the x coordinate for a KGD fracture with stress barriers at $t = t_{\text{end}}$. Colour filling indicates proppant concentration.

To establish a reference point, Fig. 2 plots the results of computations without proppant for $t = t_{\text{end}}$. The fracture width profile is shown together with the colour filling, where the latter indicates proppant concentration (which is zero in this case). Stress barriers are highlighted by grey areas, while the direction of the gravitational force is also shown. The source is located at $x = 0$, while l_1 and l_2 are the distances from the source to the left and right crack tips correspondingly. The effect of the stress barriers can clearly be seen from the Fig. 2.

To exclude the effect of gravity, first the computations for buoyant particles are considered. Fig. 3 shows the results of simulations for the reference set of parameters for different particle radii. The top pictures plot the variation of the pressure at the inlet and the half-length of the fracture (the crack is symmetric), while the centre and the bottom pictures show the corresponding width profiles at $t = t_{\text{end}}$ with colour filling showing the normalized proppant concentration. The pressure and length histories have a well-pronounced kink at $t \approx 500$ s, which corresponds to the time at which the fracture reaches the stress barriers. It is interesting to note that both the pressure and length histories have no evidence of the proppant injection at $t = 1000$ s. The proppant starts to affect the fracturing only at $t \approx 1900$ s, when it reaches the crack tip. From this time onward, different particle sizes lead to different consequences. The smallest particle size that is considered, namely $a = 0.2$ mm, causes nearly a complete arrest of the fracture and the highest pressure rise. It also leads to the widening of the crack. Bigger particles allow for the fluid filtration through the plug and thus their usage may lead to some fracture propagation even after the plug is formed. For the biggest particles, namely $a = 0.8$ mm,

the pressure rise is notably smaller than for $a = 0.2$ mm, while the length history is remarkably close to that calculated without the proppant. Particle sizes $a = 0.4$ mm and $a = 0.6$ mm represent a transition between the two extreme cases. Note that both the history of the inlet pressure and the length history feature small oscillations for times at which the proppant plug is developed. Unfortunately, as also commented in [5], this is an artifact of the numerical algorithm, which stems from the fact that the plug obeys “staircase”-like motion due to the discrete nature of the fracture width. Computations with different meshes show that the oscillations change location, but the overall trend is preserved.

Fig. 4 shows the results of simulations, analogous to that in Fig. 3, but now with weighted particles. As for Fig. 3, there is a similar hierarchy between the curves for the pressure history. However, the time instant at which the pressure starts to increase due to the formation of the proppant plug, now varies with particle size. Bigger and heavier particles settle faster, and hence initiate the formation of the plug earlier than smaller particles. The top right picture in Fig. 4 shows the histories of the distance from the inlet to the left and right crack tips for different particle radii. One can observe a complex behaviour, where the left fracture tip nearly stops for all configurations, except the one without proppant, while the response of the right tip depends significantly on the particle size. For the biggest particles considered, i.e. $a = 0.8$ mm, there is no plug formation near the right fracture tip (but the left fracture is arrested), which allows it to extend beyond the corresponding fracture without proppant (see Fig. 2). For a smaller particle size, $a = 0.6$ mm, the right crack wing (branch) first follows the path of the fracture that corresponds to $a = 0.8$ mm, while later, when the plug is formed in the right part of the fracture, it drastically changes its behaviour. The simulations with $a = 0.4$ mm exhibit qualitatively similar behaviour, although with different quantitative characteristics. For the smallest particle size, $a = 0.2$ mm, the fracture is nearly symmetric since the gravitational settling is minimal, and both left and right crack tips are significantly slowed after the initiation of the plug formation.

The considered examples show that there is a notable variability of the hydraulic fracture behaviour depending on the particle size. Gravitational settling has the largest effect, however, the fluid filtration through the proppant plug also plays an essential role. It is also important to note that both the gravitational settling and the filtration rate terms in (2) are proportional to a^2 , which causes relatively high sensitivity of the results to the particle radius.

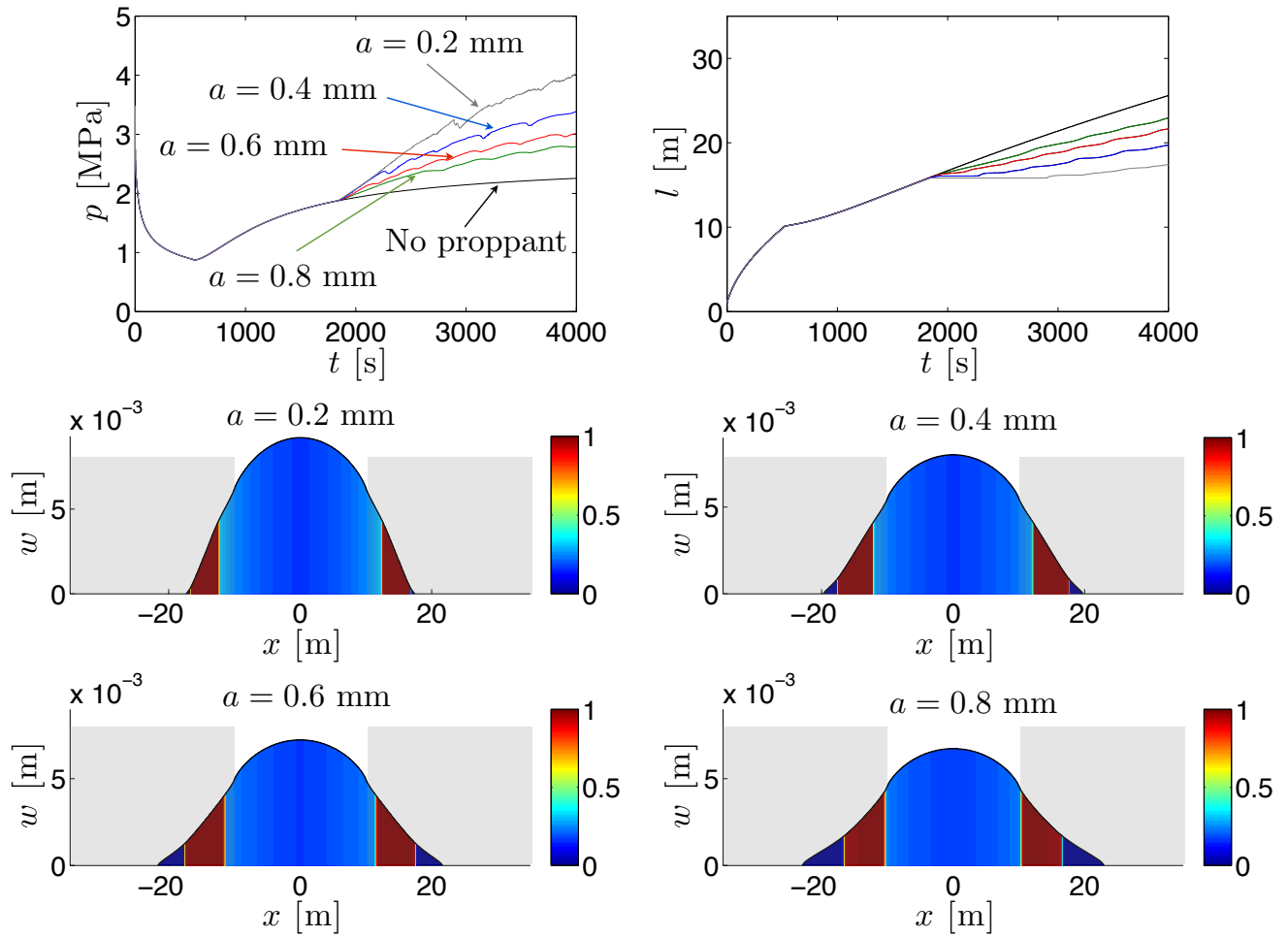


Figure 3: Results of calculations for the reference set of parameters for buoyant particles of various sizes. Top left: pressure history at the inlet $x=0$, different line colours correspond to different particle sizes. Top right: the history of the fracture half-length, defined as the distance between the inlet and the crack tip (either tip, since the fracture is symmetric). Centre and bottom: fracture width profiles for different proppant radii at $t = t_{\text{end}}$, colour indicates normalized particle concentration.

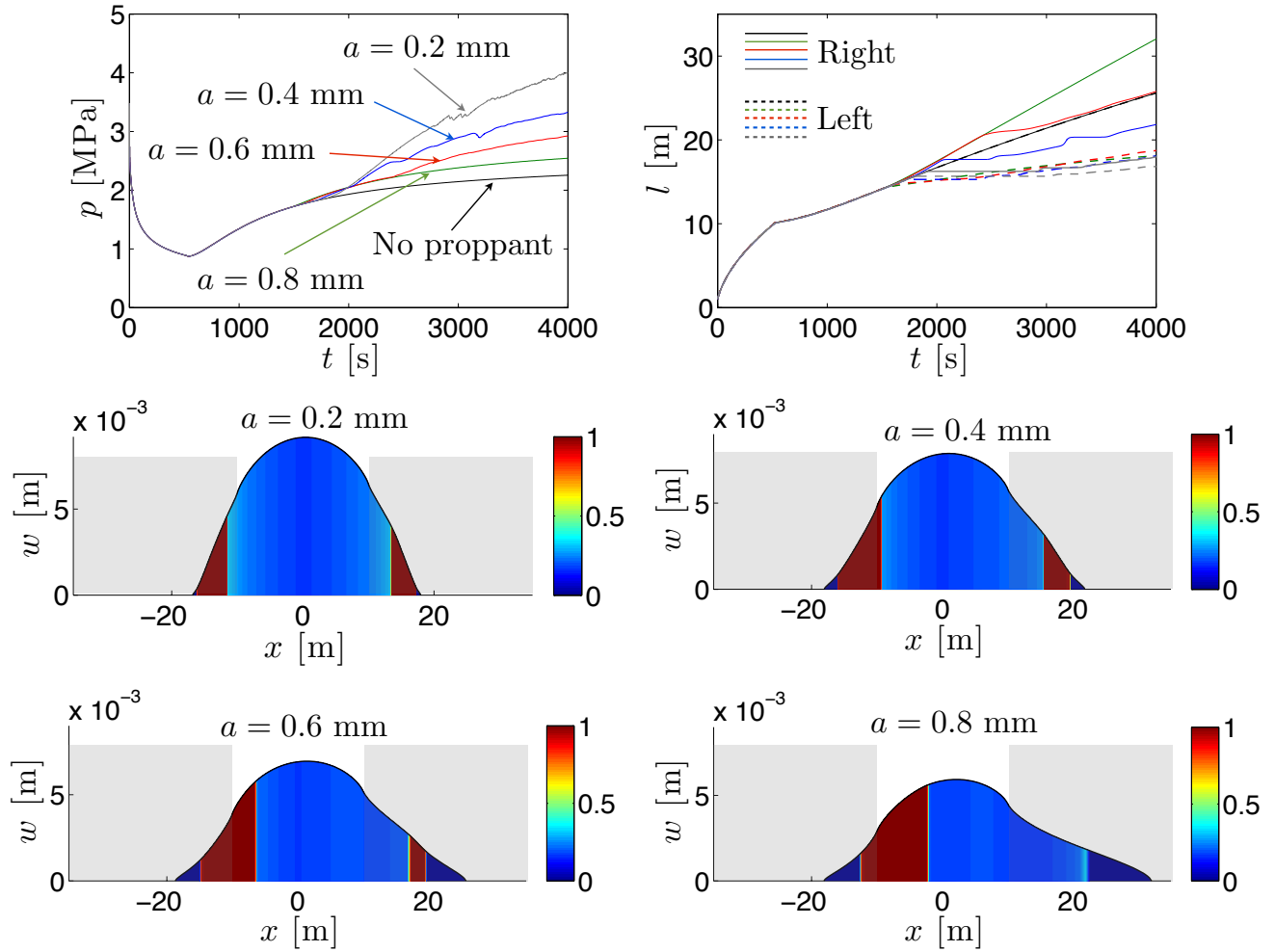


Figure 4: Results of calculations for the reference set of parameters for weighted particles of various sizes. Top left: pressure history at the inlet $x = 0$, different line colours correspond to different particle sizes. Top right: the history of the left and right fracture half-lengths, defined respectively as the distance from the inlet to the left and right fracture tips. Centre and bottom: fracture width profiles for different proppant radii at $t = t_{\text{end}}$, colour indicates normalized particle concentration.

4. EFFECTS FOR P3D FRACTURES

To study the particle size effects for a planar geometry, a P3D hydraulic fracturing model with stress barriers is considered next [14]. The numerical algorithm, that captures the proppant transport for such a geometry is described in [5]. Note that the complete formulation of the hydraulic fracturing problem is omitted here for brevity, since it can be found in [5]. As for the KGD fractures, one reference set of parameters is considered, while the particle size is varied to understand its influence. The initial condition at $t_{\text{start}} = 1$ s assumes that the fracture has an elliptic average width profile with a maximum opening $w_{\text{max}} = 10^{-3}$ m, and length of $l = 1$ m. The reference set of the problem parameters is $H = 20$ m for the width of the reservoir layer, $\mu = 0.1$ Pa·s for the intrinsic fluid viscosity, $E' = 25 \times 10^9$ Pa for the plane strain modulus, $Q_0 = 10^{-2}$ m³/s for the injection rate (source is located at $x = 0$), $\Delta\sigma = 2.5 \times 10^6$ Pa for the magnitude of the stress barriers, $K_{1c} = 10^6$ Pa·m^{1/2} for the fracture toughness, and $C' = 5 \times 10^{-5}$ m/s^{1/2} for the leak-off coefficient. Clear fluid is used for the fracturing before $t_p = 1000$ s, while after that the proppant with a normalized volume fraction $\bar{\phi}_0 = 0.2$ is pumped. All simulations end at $t_{\text{end}} = 3000$ s. Both buoyant and weighted particles are used, and, in the latter case, the difference between the particle and fluid mass densities is taken as $\Delta\rho = \rho^p - \rho^f = 1300$ kg/m³, while the gravitational acceleration is set to $g = 9.8$ m/s². Particle radii that are used for the calculations are selected within the range $0.2 \leq a \leq 0.8$ mm.

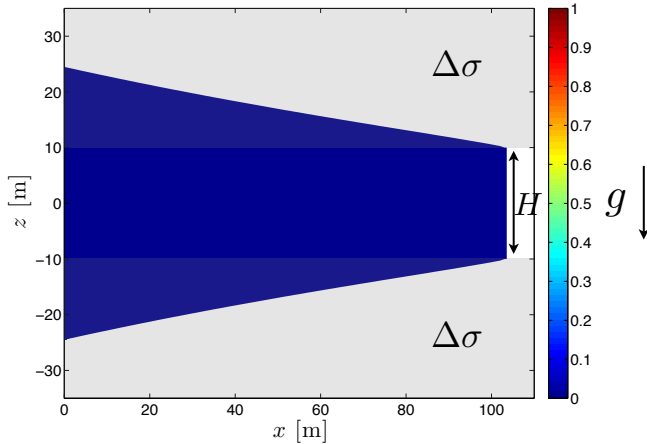


Figure 5: Fracture footprint for the P3D fracture with stress barriers at $t = t_{\text{end}}$. Colour filling indicates proppant concentration.

To specify a reference solution, Fig. 5 plots the results of calculations without proppant. The fracture footprint is shown (only half is shown due to symmetry), while the colour filling indicates the normalized proppant volume fraction. Stress barriers are highlighted by grey areas, and

the direction of gravity is also shown.

To quantify particle size effects for a P3D fracture geometry, Fig. 6 shows the results of computations for different proppant sizes for buoyant particles. The top pictures compare the histories of the fracture height at the inlet, the fracture length (i.e. the distance from the inlet to the crack tip), and the pressure at the inlet. The centre and bottom pictures show the fracture footprints for different particle sizes with the colour filling indicating the normalized proppant concentration. It is interesting to note that both the pressure and height histories are nearly identical for all particle sizes, which is not the case for the KGD fractures, see Fig. 3. At the same time, there is a variation in terms of the length histories, which has similar hierarchy as for the KGD fractures. Also note that the fracture height features a clear indication of the beginning of proppant injection at $t = 1000$ s, the pressure is affected to a smaller extent, while the length of the fracture is almost unaffected. Despite the fact that both the height and length histories show relatively small sensitivity to the particle size, the corresponding fracture footprints are notably different. When small particles block the tip region, the fracture starts to widen, but does not propagate forward. Bigger particles lead to easier fluid supply to the tip region by both filtration and the channels that form above and below the plug, which allows the fracture to advance forward even after the proppant plug is formed. It is interesting to note that the pressure rise due to proppant plug development is much smaller than for the KGD fractures, see Fig. 3. This can be explained by the fact, that once the plug is formed, the fracture still has a possibility to grow in the vertical direction and the pressure does not need to “push” the fluid through the plug or to significantly widen the crack, inducing higher elastic strains in the surrounding rock.

To include the effect of gravitational settling into consideration, Fig. 7 shows the results of calculations for weighted particles. The comparison of the variation of the height at the inlet, length of the fracture and pressure at the inlet to the corresponding curves in Fig. 6 shows that they all are nearly unaffected by settling. The fracture footprints are also almost identical, while the proppant distribution is significantly impacted by gravity. To estimate the effects of settling for a P3D fracture, the following dimensionless group is introduced in [5]

$$G_s = \frac{16\Delta\rho a^2 g Q_0 E'^3 (t_{\text{end}} - t_p)}{3\Delta\sigma^4 H^4}.$$

This parameter quantifies the ratio between the duration of proppant pumping and the time required for settling. If $G_s \gg 1$, then the settling occurs before the end of pumping, while if $G_s \ll 1$, then the effect of gravity is almost negligible. For the considered problem param-

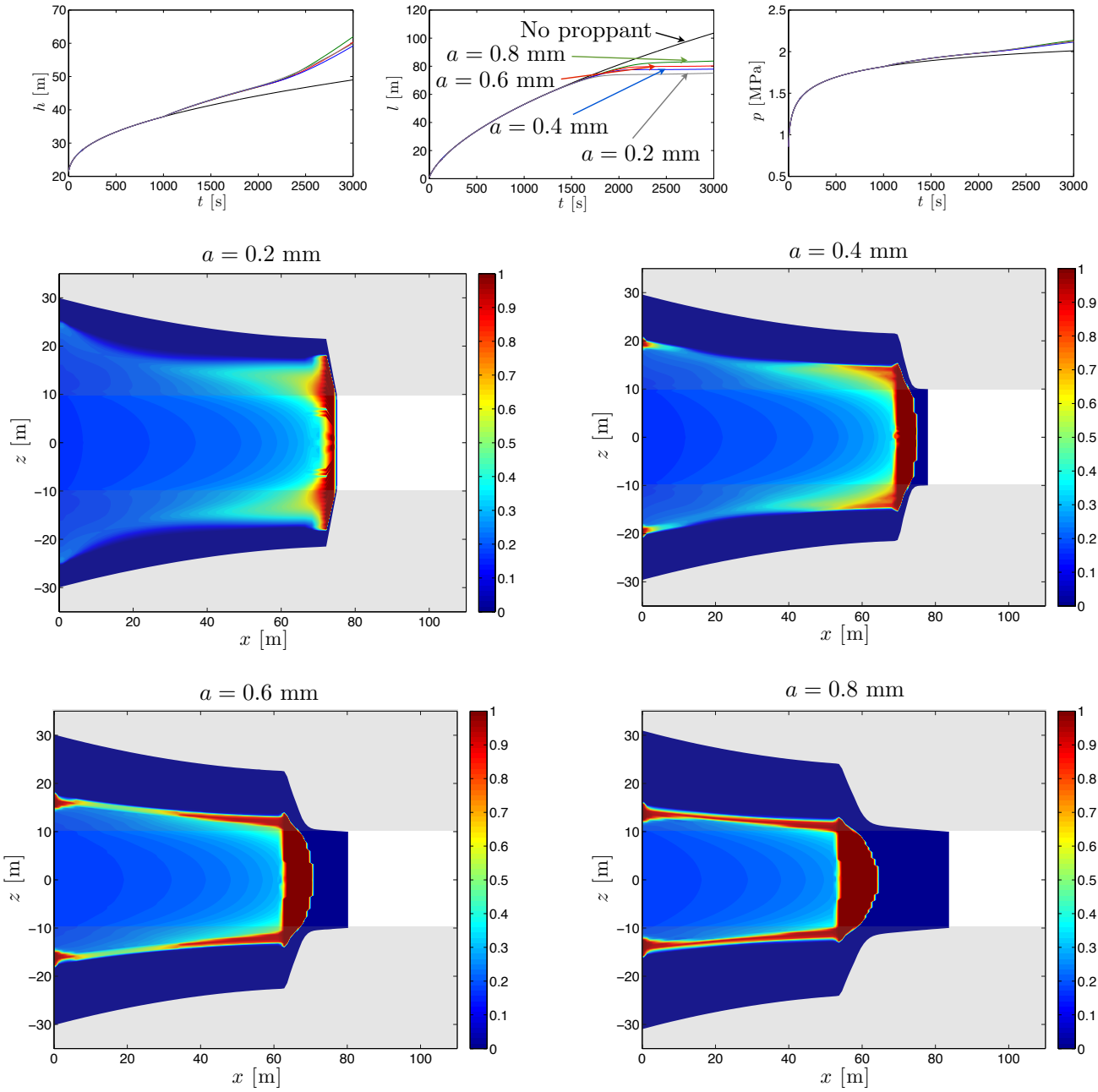


Figure 6: Results of calculations for the reference set of parameters for buoyant particles of various sizes. Top left: the history of the fracture height at the inlet $x = 0$, different line colours correspond to different particle sizes. Top centre: the history of the fracture length, defined as the distance between the inlet and the crack tip. Top right: the history of the pressure at the inlet. Centre and bottom: fracture footprints for different proppant radii at $t = t_{\text{end}}$, colour indicates normalized particle concentration.

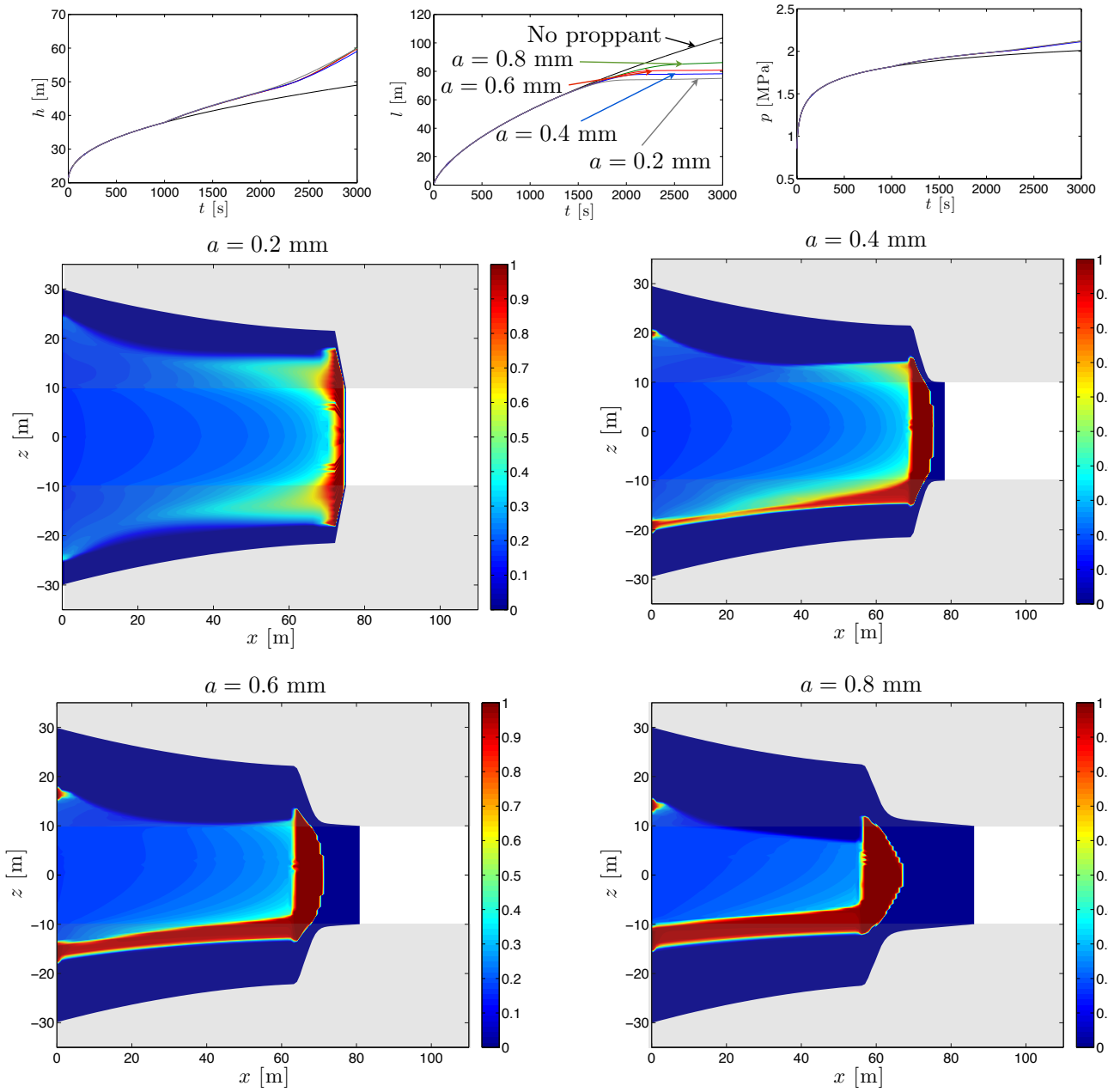


Figure 7: Results of calculations for the reference set of parameters for weighted particles of various sizes. Top left: the history of the fracture height at the inlet $x = 0$, different line colours correspond to different particle sizes. Top centre: the history of the fracture length, defined as the distance between the inlet and the crack tip. Top right: the history of the pressure at the inlet. Centre and bottom: fracture footprints for different proppant radii at $t = t_{\text{end}}$, colour indicates normalized particle concentration.

eters, $G_s = 0.14$ for $a = 0.2$ mm, $G_s = 0.54$ for $a = 0.4$ mm, $G_s = 1.2$ for $a = 0.6$ mm, and $G_s = 2.17$ for $a = 0.8$ mm. The proppant distribution in Fig. 7 is consistent with the values of G_s . Indeed, the proppant distribution is not far from being symmetric for $a = 0.2$ mm and $G_s = 0.14 \ll 1$, while higher G_s values for bigger particles lead to more pronounced asymmetry. This confirms that the dimensionless parameter G_s can be used to estimate the degree of settling *a priori*.

It is crucial to understand the limitations of the P3D model. In particular, despite the fact that the proppant transport is modelled in a 2D domain, the fracture propagation is determined by a solution of a 1D problem, which is obtained by averaging over the height of the fracture. This, together with the symmetric placement of stress barriers, implies symmetry with respect to the line $z = 0$. This is, unfortunately, not consistent with the asymmetric proppant placement caused by the gravitational settling. In other words, in situations when the settling is well-pronounced, the gravity should break the symmetry of the fracture footprint. In addition, a uniform pressure profile is assumed in each vertical cross-section, which leads to effortless fluid and proppant transport in the z direction. While this is a meaningful assumption for situations when proppant is not pumped, or its concentration is small, the horizontal plug developed for bigger particles should definitely affect the pressure distribution. It is hard to estimate the errors caused by the assumptions of the model, but one should always be aware of the limitations and possible consequences caused by the assumptions of the model.

5. SUMMARY

The goal of this study is to investigate the effects of proppant size on the hydraulic fracturing process. To analyze the aforementioned particle size effects, hydraulic fracturing simulators for KGD and P3D geometries, that account for the proppant transport, are utilized. The selected proppant transport model captures both gravitational settling and proppant plug formation near the crack tip, as well as restricts the proppant from channels whose width is smaller than the particle diameter. Two primary particle size effects are examined closely, namely the influence of settling and the consequences of fluid filtration through the proppant plug. Both phenomena are related to the square of the particle radius, which introduces a relatively high sensitivity to the particle size. By considering the propagation of KGD fractures under the same conditions, except for the different particle sizes, it is shown that both effects produce a notable influence. In particular, the gravitational settling introduces asymmetry, which may nearly arrest the downward propagation of a fracture. Simulations for buoyant particles show that the permeability of

the proppant plug affects the degree of the pressure rise after tip screen-out is achieved, showing bigger a rise for smaller particles. In addition, since the use of bigger particles promotes the fluid filtration through the plug, the fracture is able to propagate even after the plug is formed. This is not the case for smaller particles, for which the proppant plug is nearly impermeable and the fracture starts to widen once the tip screen-out is in place. Calculations for P3D fractures show both relatively small sensitivity of the inlet pressure to the particle size, and notable dependence of the fracture footprint at the same time. As for the KGD fractures, bigger particles allow for a fluid filtration through the proppant plug, which aids the fracture propagation even after the plug is formed. Small pressure sensitivity to the plug formation is related to the geometrical features of the P3D fracture, which allow for relatively compliant fracture growth in the vertical direction after the proppant has reached the tip region. Gravitational settling is shown to have a little influence on the fracture footprint even for the biggest particles considered, while the proppant placement inside the fracture is notably distorted. The lack of the fracture footprint sensitivity to the particle settling is, probably, due to the assumptions of the P3D model, which enforce the symmetry of the fracture in the vertical direction.

ACKNOWLEDGEMENTS

Authors would like to acknowledge the support of the British Columbia Oil and Gas Commission and the NSERC discovery grants program.

REFERENCES

1. Economides, M.J. and K.G. Nolte, editors. 2000. *Reservoir Stimulation*. John Wiley & Sons, Chichester, UK, 3rd edition.
2. Kuzkin, V.A., A.M. Krivtsov, and A.M. Linkov. 2013. Computer simulation of effective viscosity of fluid-proppant mixture used in hydraulic fracturing. *Comp. Phys.*, arXiv:1310.2720.
3. Mobbs, A.T. and P.S. Hammond. 2001. Computer simulations of proppant transport in a hydraulic fracture. *SPE Prod. Facil.*, 112–121.
4. Clark, P.E. 2006. Transport of proppant in hydraulic fractures. In *SPE Annual Technical Conference and Exhibition*.
5. Dontsov, E.V. and A.P. Peirce. 2014. Proppant transport in hydraulic fracturing: Crack tip screen-out in KGD and P3D models. *J. Fluid Mech. (submitted)*, <http://hdl.handle.net/2429/46109>.
6. Nolte, K.G. 1986. Determination of proppant and fluid schedules from fracturing-pressure decline. *SPE Prod. Eng.*, 255–265.

7. Gu, H. and J. Desroches. 2003. New pump schedule generator for hydraulic fracturing treatment design. In *SPE Latin American and Caribbean Petroleum Engineering Conference*.
8. Dontsov, E.V. and A.P. Peirce. 2014. A new paradigm for proppant schedule design. *HFQ (submitted)*, <http://hdl.handle.net/2429/46110>.
9. Neto, L.B. and A. Kotousov. 2013. On the residual opening of hydraulic fractures. *Int. J. Fract.*, 181:127–137.
10. Smith, M.B. and B.W. Hainey. 1997. Enhanced 2D proppant transport simulation: the key to understanding proppant flowback and post-frac productivity. In *SPE Annual Technical Conference and Exhibition*.
11. Daneshy, A.A. 2005. Proppant distribution and flowback in off-balance hydraulic fractures. *SPE Prod. Facil.*, 20:41–47.
12. Boyer, F., E. Guazzelli, and O. Pouliquen. 2011. Unifying suspension and granular rheology. *Phys. Rev. Lett.*, 107:188301.
13. Carter, E.D. 1957. Optimum fluid characteristics for fracture extension. In *Howard GC, Fast CR, editors. Drilling and production practices*, 261–270.
14. Adachi, J.I., E. Detournay, and A.P. Peirce. 2010. An analysis of classical pseudo-3D model for hydraulic fracture with equilibrium height growth across stress barriers. *Int. J. of Rock Mech. and Min. Sci.*, 47:625–639.